

Structural, electronic, and dynamical properties of calaverite AuTe₂ under pressure

Razvan Caracas and Xavier Gonze

Université Catholique de Louvain, Unité de Physico-Chimie et de Physique de Matériaux, pl. Croix du Sud 1, B-1348 Louvain-la-Neuve, Belgium

(Received 16 October 2003; published 21 April 2004)

We study from first-principles calculations the behavior of the trigonal phase of AuTe₂ under pressure, up to 75 GPa. We determine its structural evolution and predict an isosymmetrical phase transition at about 55–60 GPa, associated with a large hysteresis. We analyze the electronic properties: valence-electron-density distribution and electronic band structure. We discuss the transformations induced by the pressure in the Fermi surface, and finally determine the phonon-dispersion relations for the 50 and 75 GPa theoretical structures.

DOI: 10.1103/PhysRevB.69.144114

PACS number(s): 61.50.Ks, 63.20.Dj, 64.60.-i, 71.15.Mb

I. INTRODUCTION

Gold telluride, AuTe₂, calaverite, is incommensurately modulated at ambient conditions. Its morphology raised numerous problems to the crystallographers for a long time.^{1–4} The face-indexation problem was solved^{5,6} in 1980s, by describing the morphology and the crystal symmetry in a four-dimensional (4D) space, with a monoclinic average structure. An x-ray refinement of the incommensurate calaverite structure performed in 4D space⁷ revealed a *C2/m* average. This average phase has a distorted CdI₂ structure, each Au atom being sixfold coordinated with Te atoms, with two long and four short Au-Te bonds. The AuTe₆ octahedra form layers parallel to the (001) plane. The average phase has a metallic character.^{8–10}

The incommensurate phase is stable up to 2.5 GPa,¹¹ where it transforms to a *P3̄m1* nonmodulated trigonal phase. The trigonal phase has a less distorted CdI₂-type structure, where the six Au-Te bonds are equal. The structural evolution under pressure was recorded experimentally up to 5.4 GPa.

Interested by this pressure-driven phase transition, and building upon our previous density-functional-theory analysis,⁹ we examined the behavior of the high-pressure nonmodulated trigonal phase of calaverite under pressure, up to 75 GPa. We analyzed the structural, electronic, and dynamical properties and observed an *isosymmetrical phase transition* at about 55–60 GPa.

There are just a few compounds in nature that present such isosymmetrical phase transitions: metallic Ce (Ref. 12) and SmS (Ref. 13) that present electronic instabilities, KTiOPO₄ (Ref. 14) and PbF₂ (Ref. 15) that present structural instabilities, and Na₃MnF₆ (Ref. 16) that presents both electronic and structural instabilities. The rarity of such transitions lead us to analyze in detail the evolution not only of the structure but also of the electronic and dynamical properties under pressure of AuTe₂.

The isosymmetrical phase transition in calaverite has a first-order character and presents a calculated hysteresis of about 25 GPa. The evolution of the structure under pressure is controlled by the balance between the octahedral layer (OL) height and the interlayer (IL) distance. The driving force of the transition is the need of the structure to find its

closest possible packing. Calaverite preserves its metallic properties at high pressure. The electronic bands become more dispersive with pressure, and the Fermi surface more complex. The structures below and above the transition pressure are stable against any local or collective atomic displacement, as revealed by the phonon-dispersion relations.

The paper is organized as follows. In Sec. II we present the computational details. The structural evolution with pressure is given in Sec. III, the electronic properties are detailed in Sec. IV, and the dynamical properties in Sec. V. The paper ends with the conclusions.

II. COMPUTATIONAL METHODOLOGY

All the calculations are performed in the framework of the local-density approximation (LDA) of the density-functional theory^{17,18} as implemented in the ABINIT package.¹⁹ The ABINIT software is based on pseudopotentials and plane waves and relies on the adaptation to a fixed potential of the band-by-band conjugate-gradient method²⁰ and on a potential-based conjugate-gradient algorithm for the determination of the self-consistent potential.²¹ The pseudopotential approach is free of the spherical shape approximation used in a previous electronic structure study of calaverite.⁸ We use Hartwigsen-Goedecker-Hutter pseudopotentials²² for both elements, generated by a fully relativistic treatment (scalar relativistic as well as spin-orbit effects), due to the potential importance of relativistic effects in heavy elements. The present calculations include these effects and treat explicitly the spin-orbit effect by means of spinorial wave functions. The core configuration of Au and Te is, respectively, [Xe] and [Kr]5*d*¹⁰.

The structural relaxation was conducted using the Broyden-Fletcher-Goldfarb-Shanno minimization,²³ modified to take into account the total energy in addition to the gradients.

As usual with plane-wave basis sets, the numerical accuracy of the calculation can be systematically improved by increasing the cutoff kinetic energy of the plane waves and the density of the grid of special **k** points²⁴ used in the sampling of the Brillouin zone. The convergence of the total energy (at 1 mHa) is obtained for a 30 Ha cutoff kinetic energy of the plane waves. Then, for each value of the pressure we have consecutively increased the density of the grid

of \mathbf{k} points in order to obtain the convergence of the structural parameters (lattice constants and atomic positions). Most of the calculations are fully converged in grids of $10 \times 10 \times 10$ special \mathbf{k} points. The deviations between the residual stresses of the determined structures and the target theoretical hydrostatic pressures are less than 0.05 GPa. The calculations of the electron density and the density of states (DOS) are performed using $10 \times 10 \times 10$ grids of \mathbf{k} points. The DOS is calculated using the tetrahedron method.²⁵

The determination of the phonon-dispersion relations is done by Fourier interpolation²⁶ starting from a body-centered shifted $2 \times 2 \times 2$ grid of \mathbf{q} points in the whole Brillouin zone. The details of the dynamical matrices computation are given in Refs. 26 and 27. The calculation of the wave functions used further in the determination of the dynamical matrices are performed on $8 \times 8 \times 8$ grids of \mathbf{k} points.

The structural evolution observed in LDA was checked using also the generalized gradient approximation (GGA). The GGA calculations confirm the presence of a phase transition in the same pressure range as the LDA. This confirmation allows us to continue our study using LDA.

III. STRUCTURAL EVOLUTION UNDER PRESSURE

To start with, we examine calaverite at ambient pressure. Experimentally, calaverite has a CdI_2 -type distorted structure. The primitive unit cell contains one molecular unit. The Au atoms are situated at $(0,0,0)$ and the Te atoms at (x,x,z) and $(\bar{x}, \bar{x}, \bar{z})$ positions. The Te atoms are arranged in sheets parallel to the (001) plane with ...*ABAB*... stacking sequence. One-third of the octahedral voids between the successive *AB* Te sheets are filled by Au atoms. The resulting AuTe_6 octahedra build layers parallel to (001) . There are two apical short and four equatorial long Au-Te bonds within each octahedron.

We optimize (lattice parameters and internal atomic coordinates) the experimental average structure determined at ambient pressure. The use of Hartwigsen-Goedecker-Hutter pseudopotentials and the spin-orbit coupling improves slightly the previously obtained results¹⁰ with Troullier-Martins pseudopotentials.²⁸ We find that the energy differ-

ence between the relaxed structures with monoclinic and trigonal imposed symmetries are much lower than the accuracy of the cutoff kinetic energy and/or grid of \mathbf{k} points. So, the theoretical structure is similar to the high-pressure trigonal phase of calaverite: the deviations are less than 0.02 in the trigonal γ angle (60.00° in the ideal trigonal phase) and less than 0.0001 in the internal Te x position ($2/3$ in the ideal trigonal phase). A standard LDA calculation performed with the experimental structure gives a residual pressure of about 3 GPa. Thus, the LDA induces a pressure shift of at least 3 GPa, due to its usual volume underestimation. This gives an estimate of the accuracy of our calculations. We will focus in the following on the study of the trigonal nonmodulated phase of calaverite under pressure.

We perform first an “upward” run, which consists of relaxations under increasing pressure (with discrete steps). We use the theoretical structure obtained at the previous lower value of the pressure and make a structural optimization (unit-cell parameters and internal atomic coordinates under $P\bar{3}m1$ symmetry constraints) at a new, larger pressure. We increase the value of the pressure up to 75 GPa. We use the experimental average structure at ambient pressure to start our calculations. At 55–60 GPa a discontinuity in the evolution of the different structural parameters (a and c lattice constants, Te z coordinate, bond lengths, etc.) indicates the presence of a phase transition. As the structure preserves its symmetry, the transition is isosymmetrical, first order.

We perform next a “downward” run, which is the reverse of the previous set of calculations. We start with the 75 GPa theoretical structure and we relax it while decreasing the pressure by discrete steps. For each pressure we fully optimize the structure obtained at the previous higher value of the pressure. At about 35 to 30 GPa, the high-pressure structure reverses to the low-pressure one. The phase transition is thus associated with a hysteresis. However, our calculations are performed at 0 K, while in an experiment thermal fluctuations can overcome the energetic barrier between the two phases and the hysteresis will be temperature and time dependent.

The evolution of the lattice parameters and the Te z coordinate in the 0–75 GPa pressure range are shown, respec-

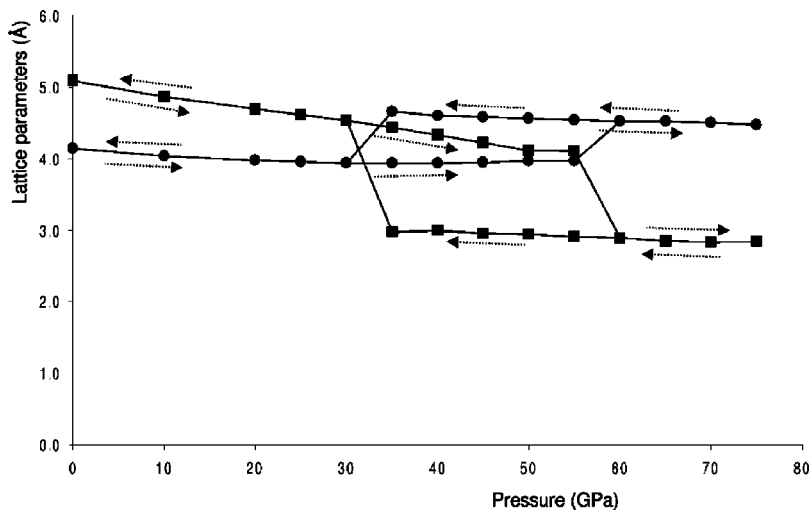


FIG. 1. Evolution of the a (circles) and c (squares) lattice parameters of calaverite under pressure.

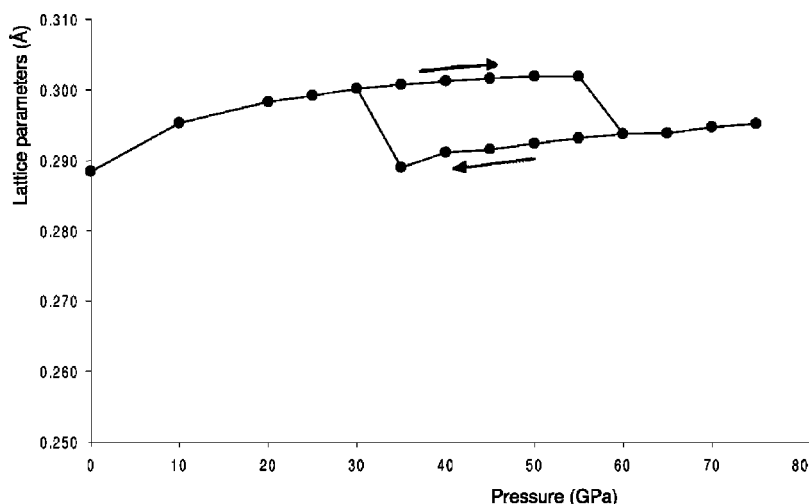


FIG. 2. Evolution of the Te z internal coordinate under pressure.

tively, in Figs. 1 and 2. The two lattice parameters behave in a highly anisotropic way at low pressure: in the 0–40 GPa range a decreases by 0.2057 Å and c by 0.7516 Å. In the 40–55 GPa pressure range a increases by 0.0265 Å, while c decreases by 0.2298 Å. After 55 GPa calaverite undergoes the phase transition, more clearly seen in the sudden decrease of the c parameter. In the high-pressure phase in the 65–75 GPa pressure range, the decrease of the a parameter, 0.0486 Å, is more important than the one of the c parameter, 0.0058 Å. During the downward run, in the 75 to 40 GPa pressure range, the lattice parameters behave more isotropically: a decreases by 0.1311 Å and c by 0.1516 Å.

The evolution of the Te z internal coordinates is such as to avoid the compression of the OL's: the Te z increases from 0.2885 at ambient pressure to 0.3019 at 55 GPa. At the phase transition it exhibits a jump to 0.2930 and increases again in the high-pressure phase. During the downward run it decreases from 0.2952 at 75 GPa to 0.2911 at 40 GPa.

The IL distance decreases by 0.4292 Å in the 0–55 GPa pressure range (representing 19.95% of the 0 GPa value), while the OL height decreases in the same pressure range by 0.3224 Å (10.99% of the 0 GPa value). During the down-

ward run the OL increases by 0.0652 Å (3.88% from its 75 GPa value), while the IL by 0.0864 Å (7.43% from the 75 GPa value).

The anisotropic behavior of the lattice parameters under pressure may be explained from the pronounced two-dimensional character of the structure. The compression of the OL's is enhanced along the [001] direction and limited within the (001) plane. The phase transition takes place at a 55–60 GPa pressure (upward run). It is marked by the sudden expansion of the structure in the (001) plane and the sudden decrease of the c parameter. The structure preserves the space group of the structure, the topology of the OL's in the (001) planes, and their packing along the [001] direction, the phase transition being isosymmetrical.

IV. ELECTRONIC PROPERTIES

A. Electron density

Figure 3 shows the valence-electron density at several pressures during the upward run. Its evolution gives an accurate image of the structural evolution. The high electron

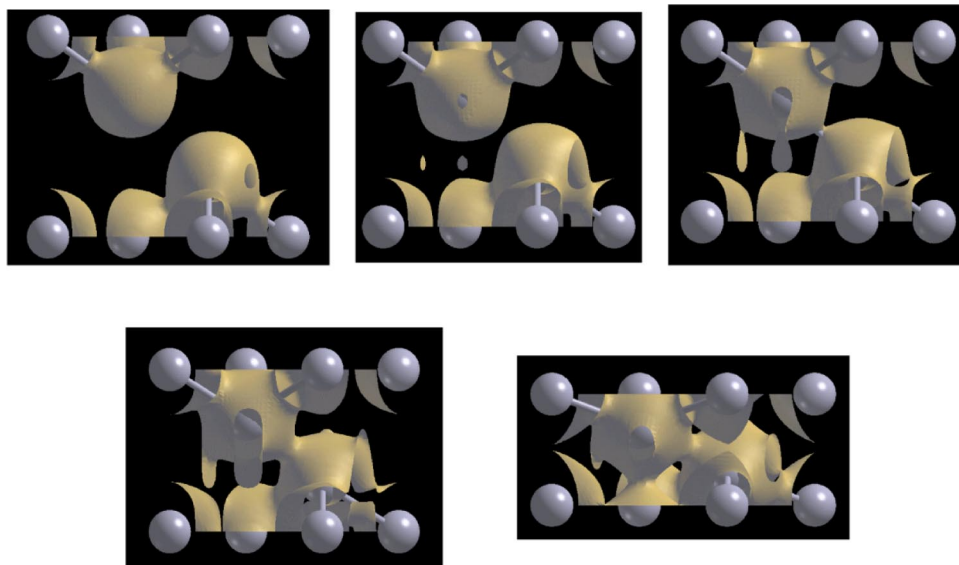


FIG. 3. (Color online) The $0.05e^-/\text{Å}^3$ isodensity surface in the theoretical structure of calaverite, computed at several pressures, during the upward run. The spheres are the Au atoms, while the Te atoms are not seen because of the isodensity surface. The first row corresponds to the 0, 20, and 30 GPa structures, and the second one to the 50 and 75 GPa pressure, respectively, from left to right.

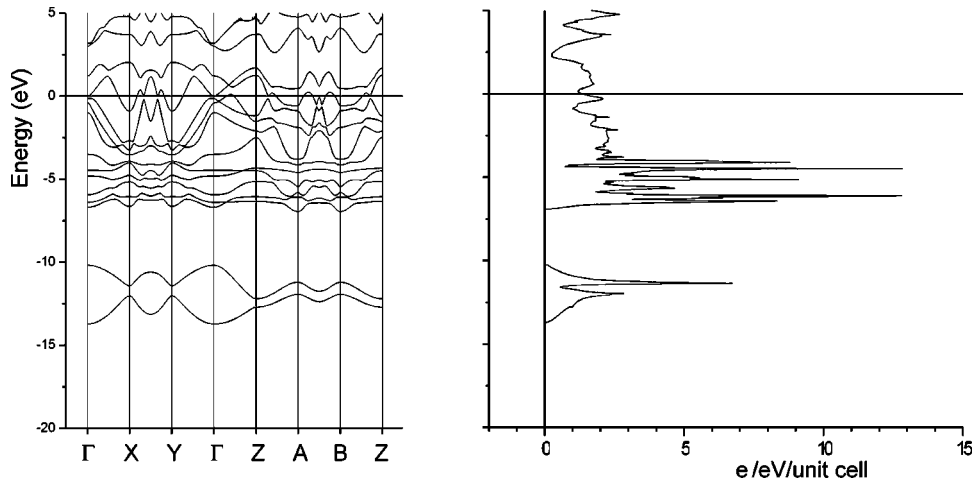


FIG. 4. The electronic band structure and the corresponding density of states for the theoretical structure at ambient pressure. Several groups of electronic bands may be distinguished. The notation of the high-symmetry points is as follows: $X=(\frac{1}{2},0,0)$, $Y=(0,\frac{1}{2},0)$, $Z=(0,0,\frac{1}{2})$, $A=(\frac{1}{2},0,\frac{1}{2})$, $B=(0,\frac{1}{2},\frac{1}{2})$.

density within the OL's (Ref. 9) limits the compression of the structure in the (001) plane. The interlayer space is relatively depleted in electrons and thus the structure may compress easily along the [001] direction. Around 40 GPa, the OL's are closer: the electronic clouds of the Te atoms in the neighboring layers exert a repulsive effect. This effect is seen in the slight increase of the a lattice parameter, which controls the extension of the layers in the (001) planes. This repulsion effect becomes sufficiently important above 50 GPa to produce the phase transition.

The electron-density distribution along the Au-Te bond remains almost constant with pressure. The highest density corresponding to the Te atom, about $0.08\text{--}0.09 e^-/\text{Ha}^3$, lies at about 0.89 \AA from the Te atomic center at all pressures. The value of the lowest density increases from $0.056 e^-/\text{Ha}^3$ (68% of the Te maximum) at 0 GPa to $0.078 e^-/\text{Ha}^3$ (86% of the Te maximum) at 50 GPa. After a sudden decrease during the phase transition (at 60 GPa it is $0.060 e^-/\text{Ha}^3$, corresponding to 72% of the Te maximum) it continues to increase with pressure. The highest density corresponding to the Au atom is almost constant in terms of both value and position: around $0.44 e^-/\text{Ha}^3$ at about $0.47\text{--}0.49 \text{ \AA}$ far from the atomic center. The minimum of the electron density along the Te-Te bond increases from $0.031 e^-/\text{Ha}^3$ at 0 GPa (39% from the Te maximum) to $0.059 e^-/\text{Ha}^3$ at 50 GPa (69% from the Te maximum). At the phase transition it

records a jump down to $0.053 e^-/\text{Ha}^3$ at 60 GPa (63% from the Te maximum). In the high-pressure phase its value increases much slowly, at 75 GPa being $0.057 e^-/\text{Ha}^3$ (67% from the Te maximum). The Te maximum, about $0.08\text{--}0.09 e^-/\text{Ha}^3$, is displaced from 0.82 \AA far from the atomic center at 0 GPa to 0.88 \AA at 50 GPa. In the high-pressure phase its position is much closer to the atomic center: 0.81 \AA at 60 GPa and 0.84 \AA at 75 GPa.

Consequently, the different compression of the OL with respect to the IL space may be directly related to the redistribution of the electron density. As the Au-Te bond lies within the OL, the small variations in the electron-density distribution along this bond are directly related to the weak compression of the OL with pressure. The electronic density varies instead more significantly along the Te-Te bond, which lies within the IL space. The pressure increases the Te-Te bond covalency (as observed in the evolution of the Te-Te minimum) during the decrease of the IL distance with pressure. The maximum values of the density around both the Te and Au atoms and also their positions do not vary considerably with pressure.

B. Electronic band structure and density of states

Figure 4 shows the electronic band structure and the corresponding DOS for the theoretical 0 GPa structure. The

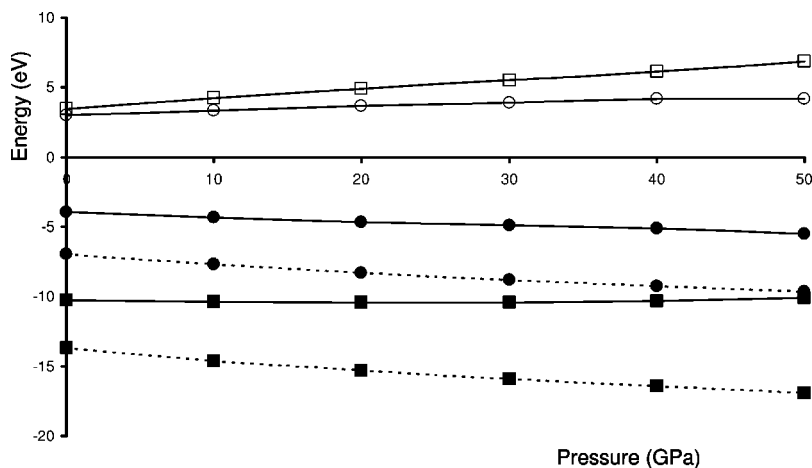


FIG. 5. The evolution with pressure of the energy limits of the two energy-lowest groups of electronic bands and the gap between them, with respect to the Fermi energy. Squares and dotted lines are for the first group, and circles and continuous lines for the second one. Full symbols are for group energy limits and open symbols for the group energy range.

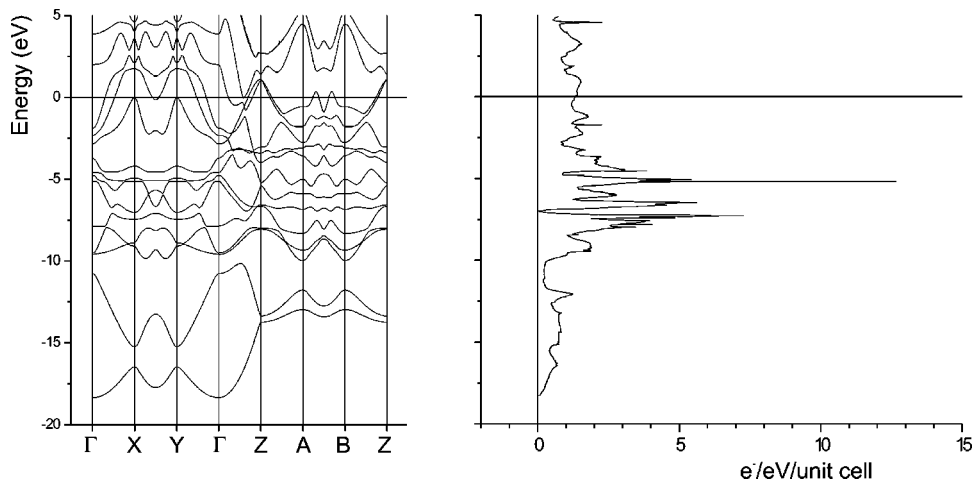


FIG. 6. The electronic band structure and the corresponding density of states for the theoretical structure at 75 GPa pressure. The bands are highly dispersive. The notation of the high-symmetry points is same as in Fig. 4.

electronic bands may be separated in several groups.⁹ The first group, the lowest in energy, is constituted of highly dispersive bands, corresponding to the Te 5*s* electrons. They span a 3.4 eV energy range. The second group is built of less dispersive bands, corresponding to the Au 5*d* electrons, that span 3 eV energy range. A 3.3 eV gap separates the first and the second groups. The third group of electronic bands is formed by highly dispersive bands, corresponding to hybrids of mainly Au 6*s*, Au 5*d*, and Te 5*p* orbitals. Its top lies 3.9 eV lower than the Fermi level. The first two conduction bands may be also contained in this group. There is no electronic gap between the second and the third group of bands.

The electronic bands become more dispersive with increasing pressure and the electrons are more delocalized. The energy width of the groups increases and the gap between the first and the second group decreases almost linearly (Fig. 5). At 50 GPa the first group of bands spans a 6.8 eV range, the second one 4.2 eV, while the gap between them is only 0.4 eV. The Fermi-level occupancy does not vary considerably with pressure.

In the high-pressure phase the electronic bands cannot be further separated (Fig. 6). The bands are highly dispersive. We observe a splitting of the Au 5*d* orbitals, possibly due to a mixing with Te 5*p* and Au 6*s* orbitals: at 6.98 eV lower than the Fermi level the DOS value reaches only about $0.0375 e^-/eV/unit\ cell$. This may be explained by the field effect induced by the Te atoms in the octahedral coordination. There are four electronic bands crossing the Fermi level in the high-pressure phase.

C. Fermi surface

The Fermi surface of the trigonal phase before the isosymmetrical transition is determined by three electronic bands that intersect the Fermi level. Figure 7(a) shows a (110) section passing through Γ through the Fermi surface in the first Brillouin zone, for the 0 GPa theoretical structure. The topology of the Fermi surface changes at 30 GPa [Fig. 7(b)], where these zones are connected along the $[11\bar{1}]$ direction. At 50 GPa pressure [Fig. 7(c)], the connecting regions become larger.

After the phase transition, the four electronic bands that intersect the Fermi level generate a very complex Fermi surface [Fig. 7(d)] with numerous electron and hole pockets.

V. DYNAMICAL PROPERTIES

Figures 8(a)–8(c) show the phonon-dispersion relations for the theoretical structures at 50 and 75 GPa. There are no unstable phonon branches: the structures are stable against any local or collective atomic displacements of weak amplitude. It is remarkable that at 50 GPa the two different structures (the low-pressure and the high-pressure ones) have stable phonon modes, indicating the (meta)stability of both.

The six optical modes in Γ may be decomposed according to the group theory as $A_{1g} + A_{2u} + E_g + E_u$. At 50 GPa (upward run) the A_{2u} , E_u , A_{1g} , and E_g modes are situated at 180, 215, 235, and 189 cm^{-1} , respectively. At 75 GPa the A_{2u} , E_u , A_{1g} , and E_g modes are situated at 78, 186, 130, and 214 cm^{-1} , respectively, while at 50 GPa (downward run) they are situated at 76, 164, 127, and 193 cm^{-1} .

The A modes correspond to vibrations along the [001]

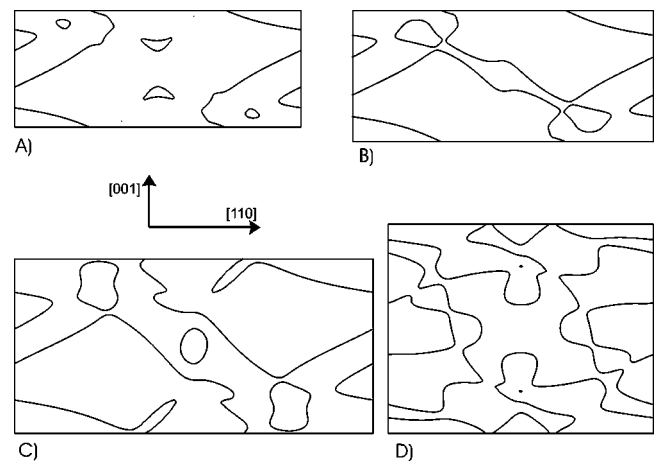


FIG. 7. (110) sections passing through Γ of the Fermi surface for the theoretical structures computed at (a) 0 GPa, (b) 30 GPa, (c) 50 GPa (upward run), and (d) 75 GPa pressures.

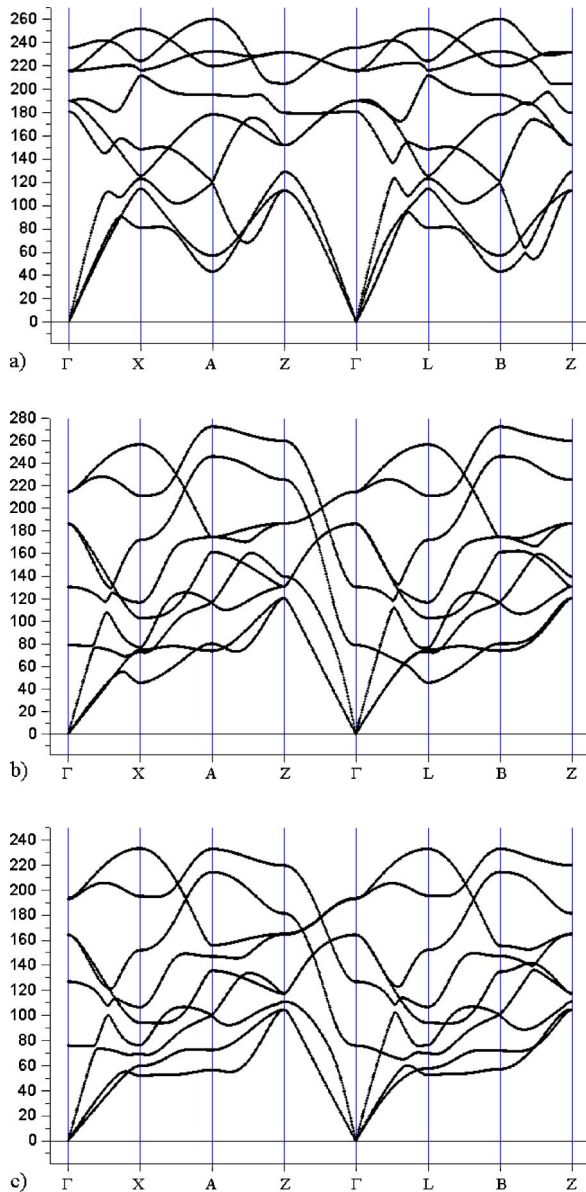


FIG. 8. Phonon-dispersion relations computed for the theoretical calaverite structures at 50 GPa during the upward run (a), 75 GPa (b), and 50 GPa during the downward run (c). The notation of the high-symmetry \mathbf{q} points is the same as in Fig. 4. $L = \frac{1}{2} \frac{1}{2} 0$. The phonon frequencies are in cm^{-1} .

direction, while the E modes to vibrations in the (001) plane. The A_{2u} mode corresponds to vibrations of the Au atoms against the Te atoms, while the A_{1g} involves only Te displacements, the two atoms in the unit cell vibrating one against the other. The E_u mode corresponds to vibrations of

both Au and Te while the E_g mode to alternate vibrations of the Te atoms around the Au atoms.

VI. CONCLUSIONS

We use the local-density approximation of the density-functional theory to study the evolution of the trigonal phase of calaverite AuTe_2 with pressure. We determine the structural and electronic properties of the calaverite in the 0–75 GPa pressure range and predict an isosymmetrical phase transition at about 55–60 GPa, characterized by a hysteresis of about 30 GPa.

Calaverite has a distorted CdI_2 -type structure: it is formed by (001) AuTe_6 octahedral layers that confers it a pronounced two-dimensional character. This character is responsible for a highly anisotropic behavior under pressure. The compression of the structure along the [001] direction is enhanced, while in the (001) plane it is limited. The phase transition has a pronounced structural character. It appears when the electrostatic repulsion between the electronic clouds of the Te atoms belonging to the neighboring layers is high enough to compensate for the Au-Te attractive interaction within the layers.

The structure has a metallic character at all pressures, but the transition generates important changes in the electronic properties. The low-pressure phase has an electronic band structure that may be separated into three groups corresponding, in increasing order of energy, to the Te $5s$, Au $5d$, and hybrids of Au $6s$, Au $5d$, and Te $5p$ electrons. The first two groups of bands get wider in energy by increasing pressure. There are three bands that intersect the Fermi level. The Fermi surface is characterized by $(11\bar{1})$ quasiplanar zones, which are separated at 0 GPa but connected after 30 GPa. The high-pressure phase has an electronic band structure built of highly dispersive bands, where the groups of bands may not be separated anymore.

We also determine the dynamical properties of the structures below and above the transition. The phonon-dispersion relations reveal stable structures both below and above the isosymmetrical phase transition.

ACKNOWLEDGMENTS

R.C. acknowledges help from computer scientists B. van Renterghem and J.-M. Beuken and interesting discussions with A. Oganov about the isosymmetrical phase transitions. X.G. acknowledges financial support from the National Fund for Scientific Research (Belgium). Support also came from the FRFC Project No. 2.4556.99 “Simulation numérique et traitement des données.”

¹H. Smith, *Miner. Mag.* **13**, 125 (1902).

²V. Goldschmidt, Ch. Palache, and M. Peacock, *Neues Jahrb. Mineral. Geol. Paleont., Ref., Beil.-Bd.* **63**, 1 (1931).

³G. Tunell and C.J. Ksanda, *J. Wash. Acad. Sci.* **26**, 507 (1936).

⁴G. Tunell and L. Pauling, *Acta Crystallogr.* **5**, 375 (1952).

⁵B. Dam, A. Janner, and J.D.H. Donnay, *Phys. Rev. Lett.* **55**, 2301 (1985).

⁶A. Janner and P. Dam, *Acta Crystallogr., Sect. A: Found. Crystal-*

- logr. **A45**, 115 (1989).
- ⁷W.J. Schutte and J.L. De Boer, *Acta Crystallogr., Sect. B: Struct. Sci.* **B44**, 486 (1988).
- ⁸B.C.H. Krutzen and J.E. Inglesfield, *J. Phys.: Condens. Matter* **2**, 4829 (1990).
- ⁹R. Caracas and X. Gonze, *Acta Crystallogr., Sect. B: Struct. Sci.* **B57**, 633 (2001).
- ¹⁰X. Gonze, R. Caracas, P. Sonnet, F. Detraux, P. Ghosez, I. Noiret, and J. Schamps, in *Fundamental Physics of Ferroelectrics 2000*, edited by Ronald E. Cohen, AIP Conf. Proc. No. **535** (AIP, Melville, NY, 2000), pp. 18–20.
- ¹¹K. Reithmayer, W. Steurer, H. Schulz, and J.L. De Boer, *Acta Crystallogr., Sect. B: Struct. Sci.* **B49**, 6 (1993).
- ¹²L.-G. Liu and W.A. Bassett, *Elements, Oxides, and Silicates: High-Pressure Phases with Implications for the Earth's Interior* (Oxford University Press, New York, 1986), p. 250.
- ¹³J.K. Burdett, *Chemical Bonding in Solids* (Oxford University Press, New York, 1995), p. 319.
- ¹⁴D.R. Alan and R.J. Nelmes, *J. Phys.: Condens. Matter* **8**, 2337 (1996).
- ¹⁵J. Haines, J.M. Leger, and O. Schulte, *Phys. Rev. B* **57**, 7551 (1998).
- ¹⁶S. Carlson, Y.Q. Yu, U. Halenius, and R. Norrestam, *Inorg. Chem.* **37**, 1486 (1998).
- ¹⁷P. Hohenberg and W. Kohn, *Phys. Rev.* **136**, B864 (1964).
- ¹⁸W. Kohn and L.J. Sham, *Phys. Rev.* **140**, A1133 (1965).
- ¹⁹X. Gonze, J.-M. Beuken, R. Caracas, F. Detraux, M. Fuchs, G.-M. Rignanese, L. Sindic, M. Verstraete, G. Zerah, F. Jollet, M. Torrent, A. Roy, M. Mikami, Ph. Ghosez, J.-Y. Raty, and D.C. Allan, *Comput. Mater. Sci.* **25**, 478 (2002).
- ²⁰M.C. Payne, M.P. Teter, D.C. Allan, T.A. Arias, and J.D. Joannopoulos, *Rev. Mod. Phys.* **64**, 1045 (1992).
- ²¹X. Gonze, *Phys. Rev. B* **54**, 4383 (1996).
- ²²C. Hartwigsen, S. Goedecker, and J. Hutter, *Phys. Rev. B* **58**, 3641 (1998).
- ²³W.H. Press, B.P. Flannery, S.A. Teukolsky, and W.T. Vetterling, *Numerical Recipes: The Art of Scientific Computing* (FORTRAN Version) (Cambridge University Press, Cambridge, 1989).
- ²⁴H.J. Monkhorst and J.D. Pack, *Phys. Rev. B* **13**, 5188 (1976).
- ²⁵P.E. Blöchl, O. Jepsen, and O.K. Andersen, *Phys. Rev. B* **49**, 16 223 (1994).
- ²⁶X. Gonze, *Phys. Rev. B* **55**, 10 337 (1997).
- ²⁷X. Gonze and C. Lee, *Phys. Rev. B* **55**, 10 355 (1997).
- ²⁸N. Troullier and J.L. Martins, *Phys. Rev. B* **43**, 1993 (1991).